Supporting Information

Extending the Experimentally Accessible Range of Spin Dipole-Dipole Spectral Densities for Protein-Cosolute Interactions by Temperature-Dependent Solvent Paramagnetic Relaxation Enhancement Measurements

Yusuke Okuno and G. Marius Clore*

Laboratory of Chemical Physics

National Institute of Diabetes and Digestive and Kidney Diseases

National Institutes of Health

Bethesda, MD 20892-0520, USA

Contents:

- 5 mathematical appendices providing derivations for various formulae in the main text
- 10 supplementary figures

SI APPENDIX

In the SI Appendix we present the mathematical derivations and underpinnings for various equations in the main text. Appendix A gives the derivation of the scaling property of the spin dipole-dipole spectral densities; Appendix B provides the relationship between the time-derivative of the correlation function and the high-frequency limit of the spectral densities; Appendix C provides the derivation of Eq. (17) of the main text that relates the high-field limit of the spectral densities and $\langle r^{-8}\rangle_{\text{norm}}$; Appendix D gives the derivation of an analytic expression for the spectral density function in the case of the non-uniform hardsphere model in the presence of a square-well potential; and finally in Appendix E, we outline the fitting procedure used for the "standard" outer- and inner-sphere model given by Eq. (26) of the main text

Appendix A. Derivation of the scaling property of the spectral densities

The scaling property of the spectral densities was first proposed by Melchior and Fries[1] and derived for the force-free hardsphere (FFHS) model.[1, 2] We briefly summarize the derivation of the scaling property in Appendix A.

We consider a cosolute and a protein that obey the Smoluchowski equation given by:[3-5]

$$\frac{\partial p\left(\vec{q},t,D_{\text{trans}}^{\text{bulk}}\middle|\vec{q}_o\right)}{\partial t}=D_{\text{trans}}^{\text{bulk}}\hat{L}p\left(\vec{q},t,D_{\text{trans}}^{\text{bulk}}\middle|\vec{q}_o\right) \tag{A1}$$

where $p\left(\vec{q},t,D_{\text{trans}}^{\text{bulk}}\middle|\vec{q}_o\right)$ is the conditional probability density of finding the cosolute at coordinate $\vec{q}$ and time t, initially located at $\vec{q}_o$, with a translational diffusion constant $D_{\text{trans}}^{\text{bulk}}$; $\vec{q}$ are the collective coordinates $\vec{q}=\{\vec{R},\hat{p},\hat{s}\}$; $\vec{R}$ is the vector pointing from the center of the protein to the center of the cosolute; $\hat{p}$ and $\hat{s}$ are the unit vectors between the center of the protein or the cosolute to the proton or electron spin, respectively. The collective vector $\vec{q}$, therefore, specifies the orientation and relative position of the protein and cosolute. The relative translational diffusion constant can be dependent on $\vec{R}$; i.e., $D_{\text{trans}}(\vec{R})$. To discriminate between $\vec{R}$-independent and -dependent relative translation diffusion constants, we define the bulk translational diffusion constant $D_{\text{trans}}^{\text{bulk}}$ as the relative translational diffusion constant when the protein and cosolute are far away from one another:

$$D_{\text{trans}}^{\text{bulk}}=D_{\text{trans,P}}+D_{\text{trans,S}} \tag{A2}$$

where $D_{\text{trans,P}}$ and $D_{\text{trans,S}}$ are the translational diffusion constants for the protein and cosolute, respectively.

The operator $\hat{L}$ is given by:

$$\hat{L} = \nabla \cdot h(R)\, e^{-\beta U(R)} \nabla\, e^{\beta U(R)} + \frac{D_{\mathrm{Rot,P}}}{D^{\mathrm{bulk}}_{\mathrm{trans}}} \nabla^{2}_{\mathrm{Rot,P}} + \frac{D_{\mathrm{Rot,S}}}{D^{\mathrm{bulk}}_{\mathrm{trans}}} \nabla^{2}_{\mathrm{Rot,S}} \tag{A3}$$

where $D_{\mathrm{Rot,P}}$ and $D_{\mathrm{Rot,S}}$ are the rotational diffusion constants for the protein P and cosolute S, respectively, and the function $h(\vec{R})$ is defined as $h(\vec{R}) = D_{trans}(\vec{R}) / D^{\mathrm{bulk}}_{\mathrm{trans}}$. The rotational Laplacian operator of the protein $\nabla^{2}_{\mathrm{Rot,P}}$ is given by:

$$\nabla^{2}_{\mathrm{Rot,P}} = \frac{1}{\sin\theta_{\mathrm{P}}} \frac{\partial}{\partial \theta_{\mathrm{P}}} \left(\sin\theta_{\mathrm{P}} \frac{\partial}{\partial \theta_{\mathrm{P}}} \right) + \frac{1}{\sin^{2}\theta_{\mathrm{P}}} \frac{\partial^{2}}{\partial \phi_{\mathrm{P}}{}^{2}} \tag{A4}$$

where θ_{P} and ϕ_{P} are the polar and azimuthal angles, respectively, of the unit vector $\hat{p}$. $\nabla^{2}_{\mathrm{Rot,S}}$ is given by Eq. (A4) by replacing the subscript P with the subscript S.

The spin dipole-dipole correlation function shown in Eq. (1) of the main text is given by:

$$C\left(t, D^{\mathrm{bulk}}_{\mathrm{trans}}\right) = n_{\mathrm{S}} \int\int \frac{P_{2}(\hat{r} \cdot \hat{r}_{o})}{r^{3} r_{o}{}^{3}} p\left(\vec{q}, t, D^{\mathrm{bulk}}_{\mathrm{trans}} \middle| \vec{q}_{o}\right) e^{-\beta U(\vec{q}_{o})}\, d\vec{q}\, d\vec{q}_{o} \tag{A5}$$

where n_{S} is the number density given by the number of cosolute molecules N_{S} divided by the sample volume V (i.e., $n_{\mathrm{S}} = N_{\mathrm{S}}/V$). The corresponding spectral density is given by:

$$J(\omega, D^{\mathrm{bulk}}_{\mathrm{trans}}) = \int_{0}^{\infty} C\left(t, D^{\mathrm{bulk}}_{\mathrm{trans}}\right) \cos(\omega t)\, dt \tag{A6}$$

It should be noted that Eq. (A6) is same as Eq. (1) of the main text except that we use the notation $J(\omega, D^{\mathrm{bulk}}_{\mathrm{trans}})$ instead of $J(\omega)$ to emphasize that the spectral density is taken when the translational diffusion constant has a value $D^{\mathrm{bulk}}_{\mathrm{trans}}$.

Let us assume that the ratios $D_{\mathrm{Rot,P}} / D^{\mathrm{bulk}}_{\mathrm{trans}}$ and $D_{\mathrm{Rot,S}} / D^{\mathrm{bulk}}_{\mathrm{trans}}$ are independent of temperature. Such an assumption is reasonable if the bulk translational and rotational diffusion constants are given by the Stoke-Einstein relations,

$$D_{\mathrm{trans,P}} = \frac{k_{B}T}{6\pi\eta R_{\mathrm{P}}}, \qquad D_{\mathrm{Rot,P}} = \frac{k_{B}T}{8\pi\eta R_{\mathrm{P}}{}^{3}} \tag{A7}$$

where R_{P} is the protein radius. The translational and rotational diffusion constants for the cosolute are given by Eq. (A7) by replacing R_{P} with R_{S}, the cosolute radius. Then the ratio of the rotational and trasnalational diffusion constants becomes:

$$D_{\mathrm{Rot,P}} / D^{\mathrm{bulk}}_{\mathrm{trans}} = \frac{3\left(R_{\mathrm{P}} + R_{\mathrm{S}}\right)}{4 R_{\mathrm{P}}{}^{3}} \tag{A8}$$

which is independent of the viscosity and temperature of the system. A similar expression holds true for the cosolute by interchanging the subscripts P and S. Further, let us assume that $h(\vec{R})$ and $e^{-\beta U(R)}$ are independent of temperature over the experimental temperature range. This assumption is rigorously valid only for the hard-sphere model where $U(R) = 0$ or ∞, but represents an approximation for real systems since β depends on temperature [i.e., $\beta = (k_B T)^{-1}$] and the potential of the mean force $U(R)$ could also be temperature dependent due, for example, to protein structural changes. Under the above assumptions, the operator $\hat{L}$ becomes independent of temperature.

Changing the independent variable from t to $\tau = D_{trans}^{bulk} t$ defines a new function given by

$$\tilde{p}(\vec{q}, \tau | \vec{q}_o) = p(\vec{q}, D_{trans}^{bulk} t, D_{trans}^{bulk} | \vec{q}_o) \tag{A8}$$

Eq. (A1) can be written as:

$$\frac{\partial \tilde{p}(\vec{q}, \tau | \vec{q}_o)}{\partial \tau} = \hat{L} \tilde{p}(\vec{q}, \tau | \vec{q}_o) \tag{A9}$$

Clearly, $\tilde{p}(\vec{q}, \tau | \vec{q}_o)$ does not explicitly depend on D_{trans}^{bulk} or temperature because none of the variables in Eq. (A9) are temperature-dependent, given the assumptions stated above. Let us define a new function $\tilde{C}(\tau)$ given by:

$$\tilde{C}(\tau) = n_S \int\int \frac{P_2(\hat{r} \cdot \hat{r}_o)}{r^3 r_o^3} \tilde{p}(\vec{q}, \tau | \vec{q}_o) e^{-\beta U(\vec{q}_o)} d\vec{q} d\vec{q}_o \tag{A10}$$

From a direct comparison of Eqs. (A5) and (A10), we observe that

$$\tilde{C}(D_{trans}^{bulk} t) = C(t, D_{trans}^{bulk}) \tag{A11}$$

Taking the Laplace transfrom of Eq. (A11), one obtains:

$$\begin{aligned} J(\omega, D_{trans}^{bulk}) &= \int_0^\infty C(t, D_{trans}^{bulk}) \cos(\omega t)\, dt \\ &= (D_{trans}^{bulk})^{-1} \int_0^\infty C(t, D_{trans}^{bulk}) \cos\left((\omega / D_{trans}^{bulk}) (D_{trans}^{bulk} t) \right) d(D_{trans}^{bulk} t) \\ &= (D_{trans}^{bulk})^{-1} \int_0^\infty \tilde{C}(\tau) \cos\left((\omega / D_{trans}^{bulk}) \tau \right) d\tau \\ &= (D_{trans}^{bulk})^{-1} \tilde{J}(\omega / D_{trans}^{bulk}) \end{aligned} \tag{A12}$$

where $\tilde{J}(\omega)$ is given by:

$$\tilde{J}(\omega) = \int_0^\infty \tilde{C}(\tau)\cos(\omega\tau)\, d\tau \tag{A13}$$

Rearranging Eq.(A12) one gets:

$$\tilde{J}\left(\omega / D_{\text{trans}}^{\text{bulk}}\right) = D_{\text{trans}}^{\text{bulk}} J\left(\omega, D_{\text{trans}}^{\text{bulk}}\right) \tag{A14}$$

or equivalently

$$\tilde{J}(\tilde{\omega}) = D_{\text{trans}}^{\text{bulk}} J\left(D_{\text{trans}}^{\text{bulk}}\tilde{\omega}, D_{\text{trans}}^{\text{bulk}}\right) \tag{A15}$$

where $\tilde{\omega} = \omega / D_{\text{trans}}^{\text{bulk}}$.

Appendix B. Relationship between the derivative of the correlation function and the high-frequency limit of the spectral density

Here we show that the first derivative of the correlation function $C(t)$ and the high-frequency limit of the spectral density are related by:[3]

$$\lim_{\omega\to\infty} \omega^2 J(\omega) = -C'(0) \tag{B1}$$

We assume that (a) $C(t)$ is a continuous function whose first, $C'(t)$, and second, $C''(t)$, derivatives are well defined; (b) $J(0) = \int_0^\infty C(t)\, dt < \infty$; and (c) $\lim_{t\to\infty} C(t) = \lim_{t\to\infty} C'(t) = 0$. Below we show that Eq. (B1) holds when the correlation function $C(t)$ satisfies the assumptions (a)-(c).

Integrating by parts Eq. (2) of the main yields the following results:

$$\begin{aligned} J(\omega) &= \int_0^\infty C(t)\cos(\omega t)\, dt = \omega^{-1} C(t)\sin(\omega t)\,\big|_0^\infty - \omega^{-1}\int_0^\infty C'(t)\sin(\omega t)\, dt \\ &= -\omega^{-1}\int_0^\infty C'(t)\sin(\omega t)\, dt \\ &= \omega^{-2} C'(t)\cos(\omega t)\,\big|_0^\infty - \omega^{-2}\int_0^\infty C''(t)\cos(\omega t)\, dt \end{aligned} \tag{B2}$$

where we assume that $\lim_{t\to\infty} C(t) = 0$ in the second line of Eq. (B2) and $\sin(\omega t) = 0$ at $t = 0$. Eq. (B2) makes sense because, from assumptions (a) and (b), integration is finite and the derivatives are well-defined. Assuming that $\lim_{t\to\infty} C'(t) = 0$, it follows that

$$\omega^{-2} C'(t) \cos(\omega t) \Big|_0^\infty = -\omega^{-2} C'(0) \tag{B3}$$

From the Riemann-Lebesgue Lemma,[6] the second term in the last equality in Eq. (B2) multiplied by ω^2 vanishes in the limit $\omega \to \infty$. Therefore,

$$\lim_{\omega\to\infty} \omega^2 J(\omega) = -C'(0) - \lim_{\omega\to\infty} \int_0^\infty C''(t) \cos(\omega t)\, dt = -C'(0) \tag{B4}$$

It is important to note that both experimental and simulated data show that the correlation function $C(t)$ for spin dipole-dipole interactions is proportional to $t^{-3/2}$ at long t.[1-3, 7-9] From this observation, it immediately follows that $\lim_{t\to\infty} C(t) = \lim_{t\to\infty} C'(t) = 0$, and hence the above analysis is expected to be valid.

Appendix C. Derivation of Eq. (17) in the main text

Here we derive the Eq. (17) which states that the high-field limit of the spectral density is approximately proportional to $\langle r^{-8} \rangle_{\text{norm}}$.

Suppose that the protein-cosolute system follows Smoluchowski Equations given by Eqs. (A1)-(A3). We can decompose the contributions from rotational and translational motions to the correlation function $C(t)$ as follows:[10-12]

$$C(t) = (4\pi) \sum_{l=0}^{\infty} \frac{(2l+4)!}{24} C_{l+2}(t) \sum_{l_1=0}^{l} \frac{p^{2(l-l_1)} s^{2l_1}}{\left(2(l-l_1)+1\right)! \left(2l_1+1\right)!} e^{-\left(\tau_{\mathrm{P},l-l_1}^{-1} + \tau_{\mathrm{S},l_1}^{-1}\right)t} \tag{C1}$$

where $\tau_{\mathrm{P},l}^{-1} = l(l+1) D_{\mathrm{Rot,P}}$ and $\tau_{\mathrm{S},l}^{-1} = l(l+1) D_{\mathrm{Rot,S}}$. $C_l(t)$ is given by

$$C_l(t) = \int_V \int_V \frac{Y_{l,0}\left(\theta_R, \phi_R\right) Y_{l,0}^*\left(\theta_{R,o}, \phi_{R,o}\right)}{R^{l+1} R_o^{\,l+1}} p\left(\vec{R}, t \middle| \vec{R}_o\right) e^{-\beta U\left(\vec{R}_o\right)} d\vec{R} d\vec{R}_o \tag{C2}$$

where $p\left(\vec{R}, t \middle| \vec{R}_o\right)$ is the conditional probability density of finding the center-to-center vector $\vec{R}$ at time t given that the vector was initially at $\vec{R}_o$, and is the solution of

$$\frac{\partial p\left(\vec{R},t\middle|\vec{R}_o\right)}{\partial t}=\nabla\cdot\left(D_{\text{trans}}(\vec{R})\,e^{\beta U(\vec{R})}\nabla\,e^{-\beta U(\vec{R})}p\left(\vec{R},t\middle|\vec{R}_o\right)\right) \tag{C3}$$

with a reflective boundary condition of

$$\hat{n}\cdot\left(D_{\text{trans}}(\vec{R})\,e^{-\beta U(\vec{R})}\nabla\,e^{\beta U(\vec{R})}p\left(\vec{R},t\middle|\vec{R}_o\right)\right)\Big|_{\vec{R}\in S}=0 \tag{C4}$$

where S denotes the surface of the protein; $\hat{n}$ is the unit vector normal to S; θ_{R} and ϕ_{R} are the polar and azimuthal angles of the unit vector $\vec{R}$; and $Y_{l,m}(\theta_{\text{R}},\ \phi_{\text{R}})$ are the corresponding spherical harmonics. It should be noted that $C_l(t)$ only depends on $\vec{R}$. It follows that $J(\omega)$ is given by

$$J(\omega)=(4\pi)\sum_{l=0}^{\infty}\frac{\left(2(l+k)\right)!}{24}\sum_{l_1=0}^{l}\frac{p^{2\left(l-l_1\right)}s^{2l_1}}{\left(2\left(l-l_1\right)+1\right)!\left(2l_1+1\right)!}\text{Re}\,j_{l+2}\left(z=i\omega+\tau_{\text{P},l-l_1}^{-1}+\tau_{\text{S},l_1}^{-1}\right) \tag{C5}$$

where $j_l(z)=\int_0^{\infty}C_l(t)\,e^{-zt}dt$; and Re $j_l(z)$ denote taking the real part of $j_l(z)$.

Consider the adjoint Smoluchowski Equation[13] of Eq.(C3) given by:

$$\frac{\partial p\left(\vec{R},t\middle|\vec{R}_o\right)}{\partial t}=e^{-\beta U\left(\vec{R}_o\right)}\nabla\cdot\left(D_{\text{trans}}(\vec{R}_o)\,e^{\beta U\left(\vec{R}_o\right)}\nabla\,p\left(\vec{R},t\middle|\vec{R}_o\right)\right) \tag{C6}$$

where the gradient operator ∇ now acts on $\vec{R}_o$. The corresponding boundary condition (cf. Eq. C4) is now given by:

$$\hat{n}\cdot\left(D_{\text{trans}}(\vec{R}_o)\,\nabla\,p\left(\vec{R},t\middle|\vec{R}_o\right)\right)\Big|_{\vec{R}_o\in S}=0 \tag{C7}$$

Let us consider the correlation function for arbitrary quantities $A(\vec{R})$ and $B(\vec{R})$ given by:

$$C_{AB}(t)=\langle A(\vec{R}(t))\,B(\vec{R}_o)\rangle=\int\int A(\vec{R})\,p\left(\vec{R},t\middle|\vec{R}_o\right)e^{-\beta U(R_o)}B(\vec{R}_o)\,d\vec{R}d\vec{R}_o \tag{C8}$$

where the integration is taken over all the accessible volume of the cosolute. We assume that $C_{AB}(t)$ goes to 0 as $t\to\infty$. Define a new function $\varphi(\vec{R}_o,t)$ given by:

$$\varphi(\vec{R}_o,t)=\int p\left(\vec{R},t\middle|\vec{R}_o\right)A(\vec{R})\,d\vec{R} \tag{C9}$$

It follows from Eq. (C7) that

$$\hat{n}\cdot D_{\text{trans}}(\vec{R}_o)\ \nabla\varphi(\vec{R}_o,t)\Big|_{\vec{R}_o\in S}=0 \tag{C10}$$

In addition, $\varphi(\vec{R}_o,t)$ satisfies the relation

$$\varphi(\vec{R}_o,t=0)=A(\vec{R}_o) \tag{C11}$$

Then it follows that:

$$\begin{aligned}
\left.\frac{dC_{AB}(t)}{dt}\right|_{t=0} &= \int\int A(\vec{R})\,B(\vec{R}_o)\left.\frac{\partial p\left(\vec{R},t|\vec{R}_o\right)}{\partial t}\right|_{t=0} e^{-\beta U(\vec{R}_o)}\,d\vec{R}\,d\vec{R}_o \\
&= \int\int A(\vec{R})\,B(\vec{R}_o)\,e^{-\beta U(\vec{R}_o)}e^{\beta U(\vec{R}_o)}\nabla\cdot\left(D_{\text{trans}}(\vec{R}_o)\,e^{-\beta U(\vec{R}_o)}\nabla p\left(\vec{R},t=0|\vec{R}_o\right)\right)d\vec{R}\,d\vec{R}_o \\
&= \int B(\vec{R}_o)\,\nabla\cdot\left(D_{\text{trans}}(\vec{R}_o e^{-\beta U(\vec{R}_o)}\nabla\varphi\left(\vec{R_0},t=0\right)\right)d\vec{R}_o \\
&= \int \nabla\cdot B(\vec{R}_o)\left(D_{\text{trans}}(\vec{R}_o)\,e^{-\beta U(\vec{R}_o)}\nabla\varphi\left(\vec{R_0},t=0\right)\right)d\vec{R}_o \\
&\quad -\int\left(\nabla B(\vec{R}_o)\right)\cdot\left(D_{\text{trans}}(\vec{R}_o)\,e^{-\beta U(\vec{R}_o)}\nabla\varphi\left(\vec{R_0},t=0\right)\right)d\vec{R}_o \\
&= -\int D_{\text{trans}}(\vec{R}_o)\,e^{-\beta U(\vec{R}_o)}\left(\nabla B(\vec{R}_o)\cdot\nabla A(\vec{R}_o)\right)d\vec{R}_o \\
&= -\langle D_{\text{trans}}(\vec{R})\,\nabla A(\vec{R})\cdot\nabla B(\vec{R})\rangle
\end{aligned} \tag{C12}$$

where we made use of Eq.(C5) in the second line, and the definition $\varphi(\vec{R}_o,t)$ given by Eq. (C9) in the third line. The vector calculus identities, given by

$$\nabla\cdot(\psi\vec{A})=\psi\nabla\cdot\vec{A}+\nabla\psi\cdot\vec{A} \tag{C13}$$

where $\vec{A}$ is any vector field and ψ is any scalar field, was used in the fourth line of Eq. (C12). Integration by parts was used in the fourth line of Eq. (C12). And finally, the divergence theorem followed by the boundary condition given by Eq. (C10) and the initial condition given by Eq. (C11) were used.

Setting $A(\vec{R})=B(\vec{R})=R^{-3}Y_{l,m}\left(\theta_R,\varphi_R\right)$, we obtain:

$$\begin{aligned}
\left.\frac{dC_{l+2}(t)}{dt}\right|_{t=0} &= -\frac{1}{2l+5}\sum_{m=-l}^{l}\int D_{\text{trans}}(\vec{R})\,e^{-\beta U(\vec{R})}\nabla\frac{Y_{l+2,m}(\hat{R})}{R^{l+3}}\cdot\nabla\frac{Y^*_{l+2,m}(\hat{R})}{R^{l+3}}d\vec{R} \\
&= -\frac{1}{2(2l+5)}\left(-\sum_{m=-l}^{l}\int D_{\text{trans}}(\vec{R})\,e^{-\beta U(\vec{R})}\frac{Y^*_{l+2,m}(\hat{R})}{R^{l+3}}\nabla^2\frac{Y_{l+2,m}(\hat{R})}{R^{l+3}}d\vec{R}\right.
\end{aligned}$$

$$+\sum_{m=-l}^{l}\int D_{\text{trans}}(\vec{R})\,e^{-\beta U(\vec{R})}\,\nabla^2\frac{Y_{l+2,m}(\widehat{R})}{R^{l+3}}\frac{Y^*_{l+2,m}(\widehat{R})}{R^{l+3}}d\vec{R}$$
$$-\sum_{m=-l}^{l}\int D_{\text{trans}}(\vec{R})\,e^{-\beta U(\vec{R})}\,\frac{Y^*_{l+2,m}(\widehat{R})}{R^{l+3}}\nabla^2\frac{Y_{l+2,m}(\widehat{R})}{R^{l+3}}d\vec{R}\Bigg)$$

$$=-\frac{1}{8\pi}\int D_{\text{trans}}(\vec{R})\,e^{-\beta U(\vec{R})}\,\nabla^2 R^{-(2l+6)}\,d\vec{R}$$
$$=-\frac{(2l+6)(2l+5)}{8\pi}\int D_{\text{trans}}(\vec{R})\,e^{-\beta U(\vec{R})}\,R^{-(2l+8)}\,d\vec{R} \tag{C14}$$
$$=-\frac{(2l+6)(2l+5)}{8\pi}\left\langle\frac{D_{\text{trans}}(\vec{R})}{R^{2l+8}}\right\rangle$$

where the relations

$$\nabla^2\frac{Y_{l,m}\left(\theta_R,\phi_R\right)}{R^{l+1}}=0 \tag{C15}$$

and

$$p_l(\widehat{R}\cdot\widehat{R})=\frac{4\pi}{2l+1}\sum_{m=-l}^{l}Y_{l,m}(\widehat{R})\,Y^*_{l,m}(\widehat{R}) \tag{C16}$$

were used in Eq. (C14), where p_l is the Legendre polynomial.

Using Eqs. (B1), (C1) and (C14), we obtain:

$$\lim_{\omega\to\infty}\omega^2 J(\omega)=15N_S\sum_{l=0}^{\infty}\frac{(2l+6)!}{6!}\sum_{l_1=0}^{l}\frac{p^{2\left(l-l_1\right)}s^{2l_1}}{\left(2l_1+1\right)!\left(2\left(l-l_1\right)+1\right)!}\left\langle\frac{D_{\text{trans}}(R)}{R^{2l+8}}\right\rangle$$
$$+N_S\sum_{l=0}^{\infty}\frac{(2l+4)!}{24}\langle D_{\text{trans}}(R)\,R^{-(l+6)}\rangle\sum_{l_1=0}^{l}\frac{p^{2\left(l-l_1\right)}s^{2l_1}\left(\tau_{\text{P},l-l_1}+\tau_{S,l_1}\right)}{\left(2l_1+1\right)!\left(2\left(l-l_1\right)+1\right)!}$$

$$=15n_S\langle D_{\text{trans}}(R)\,r^{-8}\rangle_{\text{norm}}$$
$$+n_S\sum_{l=0}^{\infty}\frac{(2l+4)!}{24}\langle D_{\text{trans}}(R)\,R^{-(l+6)}\rangle_{\text{norm}}\sum_{l_1=0}^{l}\frac{p^{2\left(l-l_1\right)}s^{2l_1}\left(\tau_{\text{P},l-l_1}+\tau_{S,l_1}\right)}{\left(2l_1+1\right)!\left(2\left(l-l_1\right)+1\right)!} \tag{C17}$$

The following relation[12] was used in Eq. (C17):

$$\langle r^{-2(k+1)}\rangle = \sum_{l=0}^{\infty} \langle R^{-2(l+k)-2}\rangle \frac{(2(l+k))!}{(2k)!} \sum_{l_1=0}^{l} \frac{p^{2(l-l_1)} s^{2l_1}}{(2l_1+1)!\,(2(l-l_1)+1)!} \tag{C18}$$

Neglecting the second term in the last equality in Eq. (C17), we obtain:

$$\lim_{\omega\to\infty} \omega^2 J(\omega) \approx 15 N_S \langle \frac{D_{\text{trans}}(\vec{R})}{r^8} \rangle \tag{C19}$$

For the force-free hard-sphere model, we get:

$$\begin{aligned}\lim_{\omega\to\infty} \omega^2 \mathrm{Re} j_{l+2}(z = i\omega + \tau_{\mathrm{P},l-l_1} + \tau_{\mathrm{S},l_1}) = \\ 4\pi D_{\text{trans}} R_C^{-(2l+5)} \Bigg[(l+3) + \frac{R_C^2}{(2l+3) D_{\text{trans}}} \left(\tau_{\mathrm{P},l-l_1} + \tau_{\mathrm{S},l_1} \right) - \sqrt{\frac{D_{\text{trans}}}{2R_C^2}} (l+3)^2 \omega^{-1/2} \\ - \frac{1}{2\sqrt{2}} \left(\frac{D_{\text{trans}}}{R_C^2} \right)^{3/2} (l+3)^2 \left((l+4)(l+1) D_{\text{trans}} + 5R_C^2 \left(\tau_{\mathrm{P},l-l_1} + \tau_{\mathrm{S},l_1} \right) \right) \omega^{3/2} + O(\omega^{5/2}) \Bigg]\end{aligned} \tag{C20}$$

Substituting Eq. (C20) into Eq. (C5) yields the analytic expression for $\omega^2 J(\omega)$. The analytic expression of $\langle r^{-8}\rangle_{\text{norm}}$ is given by substituting $k = 3$ in Eq. (C18):

$$\langle r^{-8}\rangle_{\text{norm}} = \frac{\left(-15p^8 + 4p^6 \left(9R_C^2 - 5s^2 \right) + 3\left(R_C^2 - s^2 \right)^3 \left(3R_C^2 + 5s^2 \right) - 2p^4 \left(9R_C^4 + 34R_C^2 s^2 - 35s^4 \right) - 4p^2 \left(R_C^2 - s^2 \right) \left(3R_C^4 - 22R_C^2 s^2 - 5s^4 \right) \right)}{45 R_C^{-3} \left(\left((p-s)^2 - R_C^2 \right) \right)^4 \left(\left((p+s)^2 - R_C^2 \right) \right)^4} \tag{C21}$$

Appendix D. The spectral density for the non-uniform diffusion hardsphere model with a square potential

An analytic expression for the spectral density for non-uniform diffusion hardsphere model in the presence of the square well potential was derived by Frezzato et al.[3] Here we summarize their findings.

The square-well potential model is defined by:

$$e^{-\beta U(R)} = \begin{cases} \alpha \text{ if } R_C \le R < R_b \text{ (region 1)} \\ 1 \text{ if } R_b \le R \text{ (region 0)} \end{cases} \tag{D1}$$

where α is the Boltzmann factor, R_C is the contact distance, and R_b is the boundary of the local domain (see Fig. 2 of the main text). Frezzato et al.[3] found an analytical expression for the square-well model with translational diffusion constants $D^{(n)}_{\text{trans}}$ and n = 1 or 0 depending on whether cosolute is in region 1 or 0. This notation corresponds to the local and bulk domains in the current work. The result is reproduced here:

$$j_l(z) = \frac{1}{VD^{(0)}_{\text{trans}} {R_C}^{2l-3}} \frac{1}{{\zeta_0}^2} \left(\frac{\alpha + (1-\alpha)\lambda^{2l-1}}{2l-1} + \alpha\lambda^{l-1}\zeta_1 Q_{l-1}(ik) \right.$$
$$\left. - \frac{1}{T^k_l} \left\{ \lambda^{2l-2}\zeta_0 k_{l-1}(\zeta_0/\lambda) X_l + \alpha \left[\zeta_1 Y_l - 2\frac{\lambda^{l+1}}{\zeta_0} k_{l-1}(\zeta_0/\lambda) \right] V_l \right\} \right) \tag{D2}$$

where

$$\zeta_n = \sqrt{\frac{z{R_C}^2}{D^{(n)}_{\text{trans}}}}, \qquad \lambda = \frac{R_C}{R_b}, \qquad \gamma = \sqrt{\frac{D^{(0)}_{\text{trans}}}{D^{(1)}_{\text{trans}}}},$$

i_l and k_l are the modified spherical Bessel functions of the first and second kind. The derivatives of i_l and k_l are defined by $i'_l(\xi) = \left.\frac{\partial i_l(y)}{\partial y}\right|_{y=\xi}$ and $k'_l(\xi) = \left.\frac{\partial k_l(y)}{\partial y}\right|_{y=\xi}$.

$$Q_{l-1}(ik) = i_{l-1}(\zeta_1) k_{l-1}(\zeta_1/\lambda) - k_{l-1}(\zeta_1) i_{l-1}(\zeta_1/\lambda)$$
$$S^{kk}_l = \gamma k'_l(\zeta_0/\lambda) k_l(\zeta_1/\lambda) - \alpha k_l(\zeta_0/\lambda) k'_l(\zeta_1/\lambda)$$
$$S^{ki}_l = \gamma k'_l(\zeta_0/\lambda) i_l(\zeta_1/\lambda) - \alpha k_l(\zeta_0/\lambda) i'_l(\zeta_1/\lambda)$$
$$S^{ik}_l = \gamma i'_l(\zeta_0/\lambda) k_l(\zeta_1/\lambda) - \alpha i_l(\zeta_0/\lambda) k'_l(\zeta_1/\lambda)$$
$$S^{ii}_l = \gamma i'_l(\zeta_0/\lambda) i_l(\zeta_1/\lambda) - \alpha i_l(\zeta_0/\lambda) i'_l(\zeta_1/\lambda)$$
$$T^k_l = k'_l(\zeta_1) S^{ki}_l - i'_l(\zeta_1) S^{kk}_l$$
$$T^i_l = k'_l(\zeta_1) S^{ii}_l - i'_l(\zeta_1) S^{ik}_l$$
$$U^k_{l-1} = k_{l-1}(\zeta_1) - \lambda^{l-1} k_{l-1}(\zeta_1/\lambda)$$
$$U^i_{l-1} = i_{l-1}(\zeta_1) - \lambda^{l-1} i_{l-1}(\zeta_1/\lambda)$$
$$V_l = k'_l(\zeta_1) U^i_{l-1} + i'_l(\zeta_1) U^k_{l-1}$$
$$X_l = i_{l-1}(\zeta_0/\lambda) T^k_l + k_{l-1}(\zeta_0/\lambda) T^i_l$$
$$Y_l = S^{kk}_l U^i_{l-1} + S^{ki}_l U^k_{l-1}$$

For $\alpha = 1$ and $\gamma = 1$, we obtain the FFHS spectral densities given by[19]

$$j_l(z) = \frac{1}{VD_{\text{trans}}R_C^{2l-3}} \frac{1}{\zeta^2}\left(\frac{1}{2l-1} - \frac{l+1}{\zeta^2}\left[1 + \frac{l+1}{\zeta}\frac{K_{l+1/2}(\zeta)}{K_{l-1/2}(\zeta)}\right]^{-1}\right) \tag{D3}$$

where $\zeta = \sqrt{\frac{zR_C^2}{D_{\text{trans}}}}$ and $K_l(x)$ is the modified Bessel function of the second kind.

Appendix E. Data fitting procedure for the outer- and inner- sphere model

Instead of parameterizing the contact distance R_C, the relative translation diffusion coefficient D_{trans} and the spin dipole-dipole correlation time τ_{in} for the bound cosolute, we define the following 3 parameters:

$$\begin{aligned} k_1 &= \frac{16\pi n_S}{27 D_{\text{trans}} R_C J(0)} \\ k_2 &= D_{\text{trans}}^{-3} \\ k_3 &= \tau_{\text{inner}} \end{aligned} \tag{E1}$$

Using the above definitions of k_1, k_2, and k_3, the σ term that appears in Eq. (24) of the main text can be expressed as:

$$\sigma = \frac{16\pi n_S}{27 k_1 J(0)}\sqrt{2\omega k_2} \tag{E2}$$

We also define new fitting functions given by:

$$j_{\text{FFHS}}(\omega) = \frac{J_{\text{FFHS}}(\omega)}{J(0)} \tag{E3}$$

$$j_{\text{inner}}(\omega) = \frac{1}{1 + (\omega k_3)^2} \tag{E4}$$

The fitting function defined in Eq. (26) of the main text can then be expressed as:

$$J_{\text{in+out}}(\omega) = J(0)\left(j_{\text{FHHS}}(\omega) + \left(1 - k_1\right) j_{\text{inner}}(\omega)\right) \tag{E5}$$

Using Eq. (E5) for fitting the experimental data rather than Eq. (23) in the main text has the advantage that the parameters k_1, k_2, and k_3 are more convenient than R_C, D_{trans} and τ_{inner} since k_1 can be restrained to range from 0 to 1. As a result, Eq. (E5) is guaranteed to satisfy the relation $J_{\text{in+out}}(0) = J(0)$. We also found that parameterizing k_2 is more practical than parameterizing D_{trans}. We can easily convert k_2 into D_{trans} by simply taking the -1/3 power of k_2. R_C and C_{inner} are given by:

$$R_C = \left(\frac{16\pi n_S}{27J(0)}\right) k_1^{-1} k_2^{-1/3} \tag{E5}$$

$$C_{\text{inner}} = J(0)\,\frac{1 - k_1}{k_3} \tag{E6}$$

Next, we derive Eq. (27) of the main text. Using Eq. (8) in the main text, we get

$$\langle r^{-6}\rangle_{\text{norm}}^{\text{Eq.(26)}} = \frac{2}{n_S\pi}\int_0^{\infty} J_{\text{FHHS}}(\omega)\,\mathrm{d}\omega + \frac{2}{n_S\pi}\int_0^{\infty} J_{\text{inner}}(\omega)\,\mathrm{d}\omega \tag{E7}$$

The first term in Eq. (E7) involves integration of Eq. (24) of the main text from 0 to ∞. Instead of evaluating the integral directly, we used the fact that the center-to-center FFHS model describes the hard sphere model with nuclear and electron spins at their respective centers and $\langle r^{-6}\rangle_{\text{norm}}$ for the center-to-center FFHS model is given by $4\pi/3R_C^3$; we get

$$\frac{2}{n_S\pi}\int_0^{\infty} J_{\text{FFHSt}}(\omega)\,\mathrm{d}\omega = \frac{4\pi}{3R_C^3} \tag{E8}$$

For the second term in Eq. (E7), we use the relation

$$\int_0^{\infty} \frac{\tau_{\text{in}}}{1 + \left(\omega\tau_{\text{in}}\right)^2}\mathrm{d}\omega = \frac{\pi}{2} \tag{E9}$$

The direct evaluation of the integral of Eq. (25) yields

$$\frac{2}{n_S\pi}\int_0^{\infty} J_{\text{inner}}(\omega)\,\mathrm{d}\omega = C_{\text{inner}} \tag{E10}$$

Eq. (27) in the main text follows from adding Eqs. (E8) and (E10).

Finally, we derive Eq. (28) of the main text. It is easy to see that the high-frequency limit of Eq. (25) in the main text is given by:

$$\lim_{\omega \to \infty} \omega^2 J_{\text{inner}}(\omega) = \frac{n_S C_{\text{inner}}}{\tau_{\text{in}}} \tag{E11}$$

For the center-to-center FFHS model (i.e., $p = s = 0$), the only term that is nonvanishing is $l = 0$. Substituting Eq. (C20) with $l = 0$, one obtains:

$$\lim_{\omega \to \infty} \omega^2 J_{\text{FFHS}}(\omega) = \frac{n_S 12\pi D_{\text{trans}}}{R_C{}^5} \tag{E12}$$

Summing Eqs. (E11) and (E12), followed by substitution into Eq. (17) in the main text, yields Eq. (27) in the main text.

Supplimentary Figures

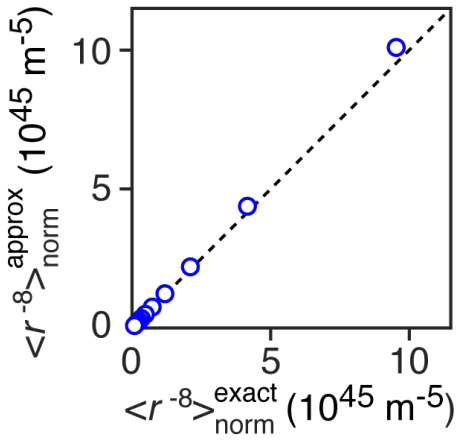

Figure S1. Comparison between exact $< r^{-8} >^{\text{exact}}_{norm}$ and approximate $< r^{-8} >^{approx}_{norm}$ values (see Eq. 17 of the main text). $< r^{-8} >^{approx}_{norm}$ and $< r^{-8} >^{\text{exat}}_{norm}$ were calculated using Eqs. (C19) and (C20), respectively. The radii of the protein (R_P) and paramagnetic cosolute (R_S) were set to 16.2 and 3.5 Å, respectively; the contact distance was set to $R_C = R_P + R_S$; T = 298 K, η = 0.89 cp, and $n_S = 1\ m^{-3}$. The distance of the nuclear spin from the center of the protein was varied from 0.6 to 14.8 Å, while the electron spin on the cosolute was fixed with s = 2.0 Å.

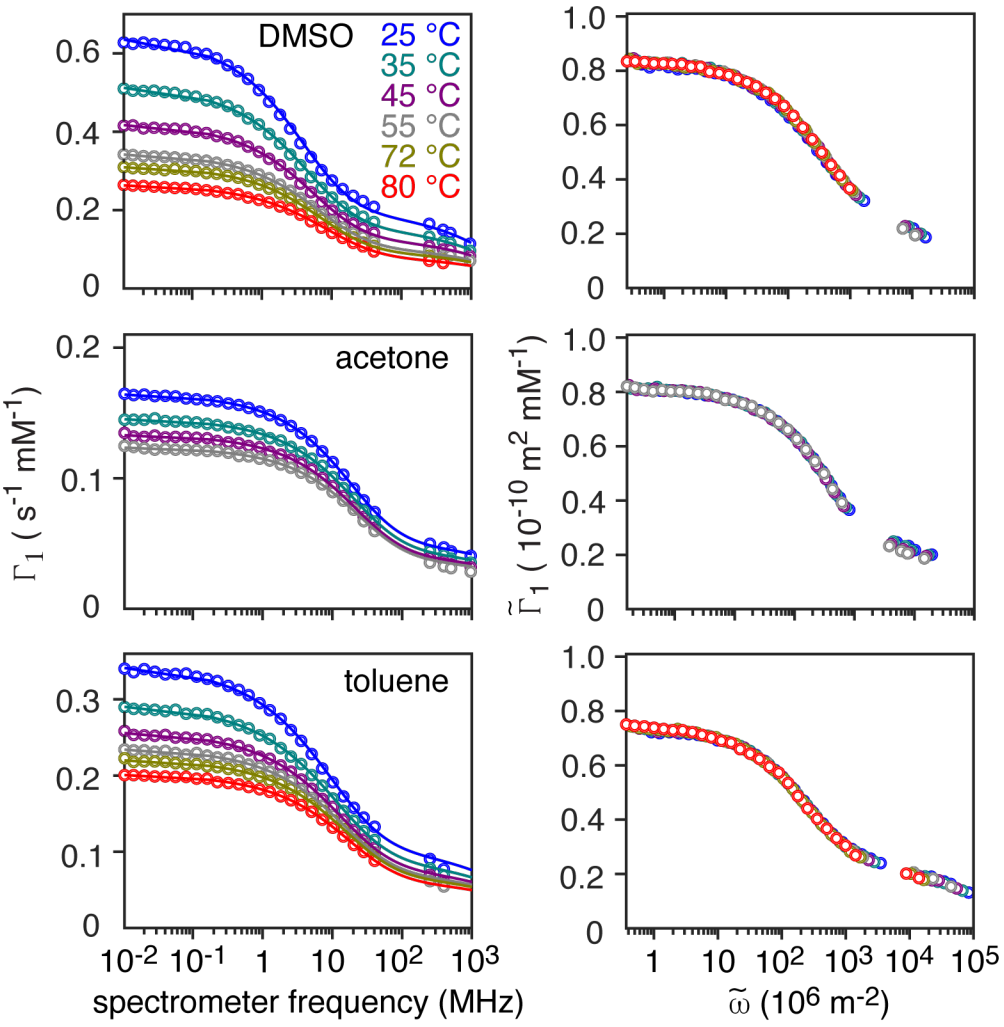

Figure S2. The scaling property holds for nuclear magnetic relaxation dispersion (NMRD) ^{1}H-Γ_1 relaxivity profiles measured for DMSO, acetone and toluene in the presence of the nitroxide radical TEMPOL at ^{1}H Larmor frequencies ranging from 0.01 to 950 MHz and temperatures spanning 25 to 80 °C. Each NMRD profile at a given temperature was fitted using Eqs. (3) and (9) from the main text. The fitted curves are shown as continuous lines in the left-hand panels. The scaling property was applied using Eq. (22) combined with Eq. (3) from the main text for each temperature, and the results are displayed in the right-hand panels. The NMRD data and the translational diffusion constants for DMSO, acetone and toluene at given tempeature were obtained from Neugebauer et al.[14]

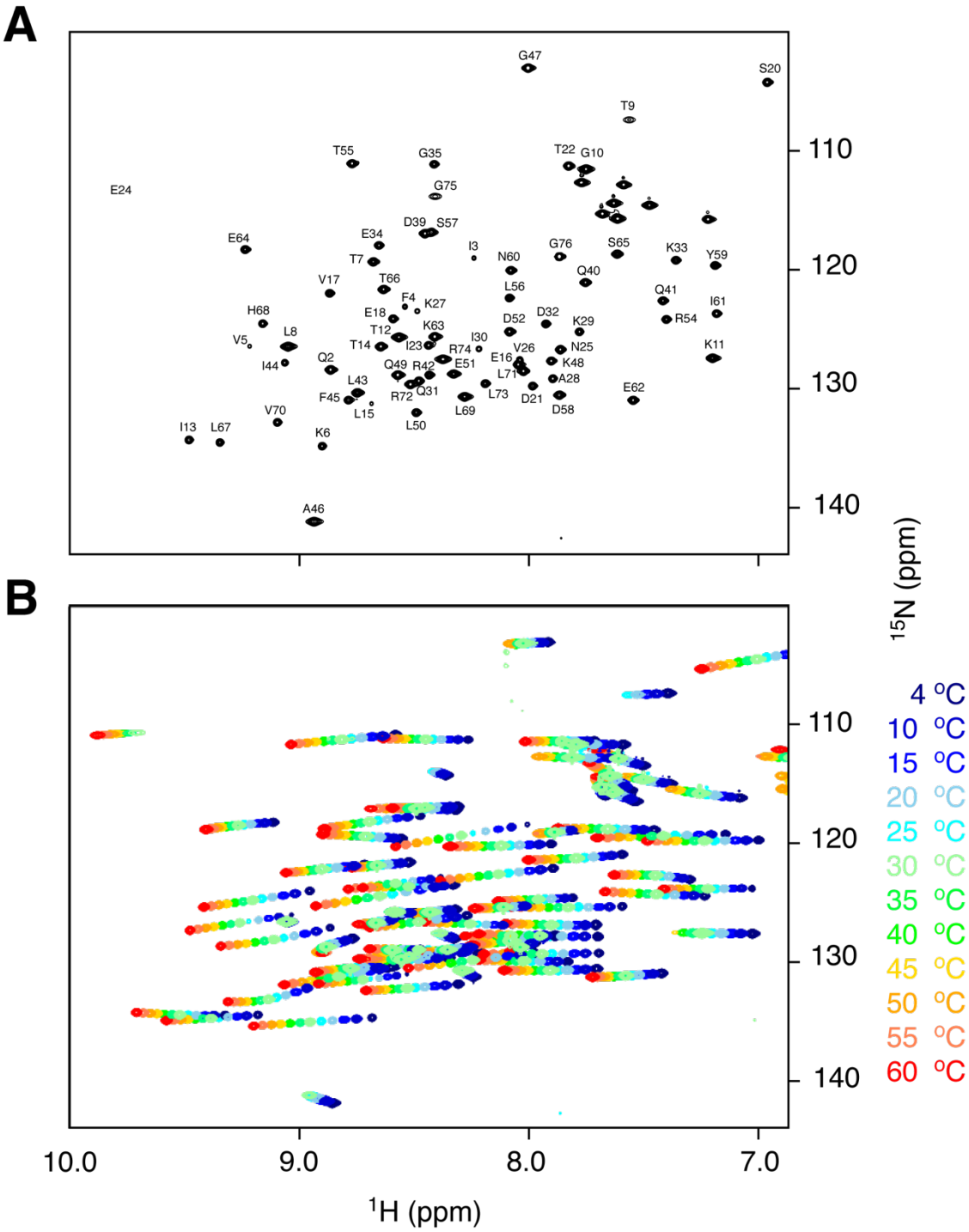

Figure S3 Temperature dependence of ^{1}H-^{15}N HSQC spectra of ubiquitin over a temperature range spanning from 4 to 60 ºC. (A) ^{1}H-^{15}N HSQC of ubiquitin at 25 °C with cross-peak assignments labeled. (Note the cross-peak for E24 is only observed at temperatures of 40 °C and higher. The assignments were based on refs. [15, 16]. (B) Overlay of the ^{1}H-^{15}N HSQC spectra at various temperatures ranging from 4 to 60°C. Thecross-peaks are colored according to the temperature as indicated on the right-hand side of the figure. All spectra were collected at 500 MHz and pH 7.0.

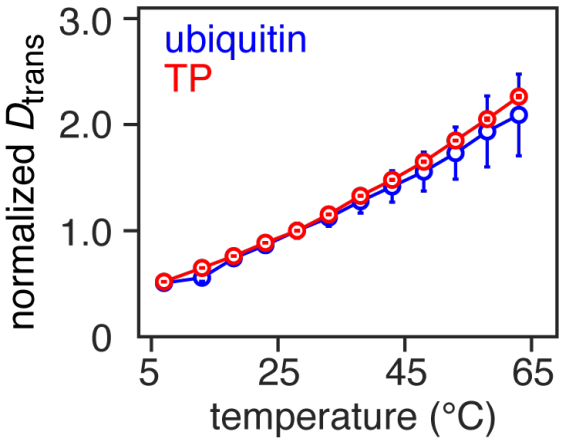

Figure S4. Temperature dependence of the normalized translational diffusion constant (D_{trans}) for ubiquitin and 2,2,5,5-Tetramethyl-3-pyrroline-3-carboxamide (TP). The translational diffusion constants were measured using pulse-field-grandient (PFG) NMR diffusion experiments. The data on TP were used to estimate the translational diffusion constants for 3-carbamoyl and 3-carboxy PROXYL. The values of D_{trans} were normalized to their respective D_{trans} values at 25 °C.

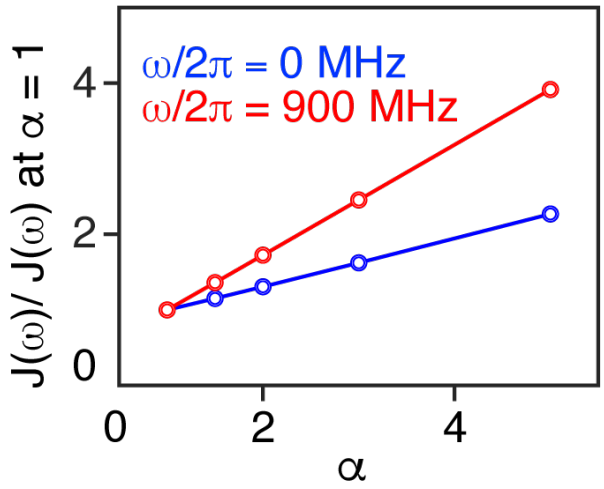

Figure S5. Impact of local intermolecular interactions on $J(\omega)$ when $\omega/2\pi = 0$ and 900 MHz. The square-well potential with a hard-sphere defined in Eq. (D1) was used in the simulation. The ratio of $J(\omega)$ to $J(\omega)$ when $\alpha = 1$ is plotted as a function of the Boltzmann factor α (see Eq. D1) . The spectral densities at static spectrometer fields of 0 and 900 MHz were generated from Eq. (D2) with the radii for the protein (R_P) and paramagnetic cosolute (R_S) set to 16.2 and 3.5 Å, respectively; the contact distance was set to $R_C = R_P + R_S$; $T = 298$ K, $\eta = 0.89$ cp, and $n_S = 1\ m^{-3}$. The distance of the nuclear and electron spins from the protein and paramagnetic cosolute centers, respectively were set to $p = 13.7$ Å and $s = 2.0$ Å. The boundary R_b of the local domain (see Fig. 2 in the main text) was set to 3.0 Å.

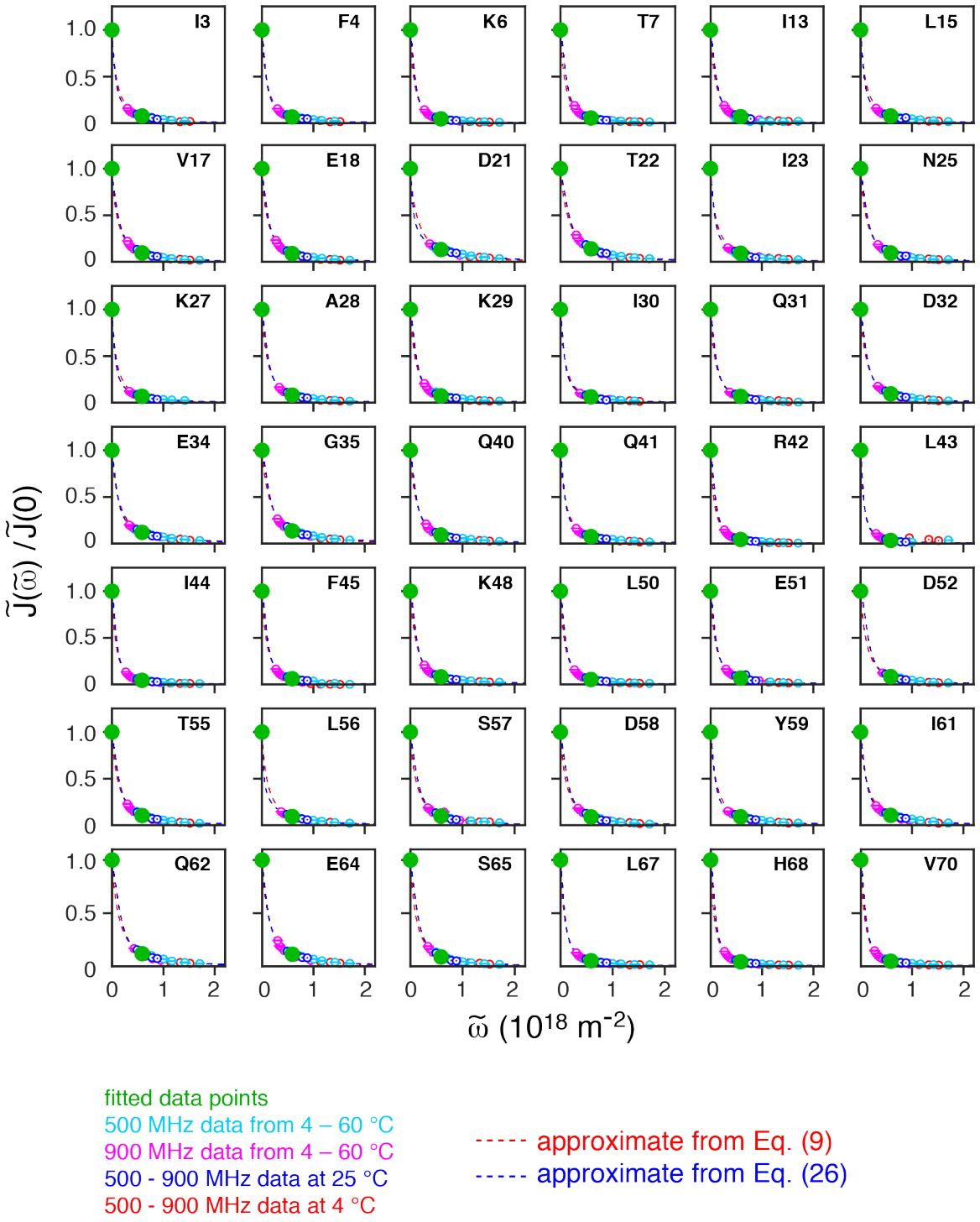

Figure S6. $\tilde{J}(\tilde{\omega})$ for residues of ubiqutin in the presence of 3-carbamoyl PROXYL using scaling property given by Eq. (22) of the main text. The $\tilde{J}(\tilde{\omega})$ values are obtained from the experimental ^{1}H-Γ_1 values measured over a temperature of 4 to 50 °C at several spectrometer frequencies. The $J(0)$ values were calculated from the experimental ^{1}H-Γ_2 and ^{1}H-Γ_1 values measured at 25 °C and 600 MHz (green filled-in

Figure S6 legend (cont.)

circles). The $J(0)$ and $J(\omega_H)$ values at 600 MHz (green filled-in circles) were used for fitting using Eqs. (9) (red dashed curve) or (26) (blue dashed curve). The magenta and cyan circles represent the $\tilde{J}(\tilde{\omega})$ calculated from the experimental ^{1}H-Γ_1 values measured at 500 and 900 MHz over a temperature range of 4 to 50 °C. The red and blue circles represents the $\tilde{J}(\tilde{\omega})$ calculated from the experimental ^{1}H-Γ_1 values measured at 4 and 25 °C at spectrometer frequencies of 500, 600, 700, 800 and 900 MHz. Note that the red and blue circles overlay almost completely with the magenta and cyan circles, and therefore may not be clearly visible in this plot. The data points that deviate significantly from the scaling property (i.e., the points for which the cyan and magenta circles at 500 and 900 MHz do not overlay) have been removed in these plots.

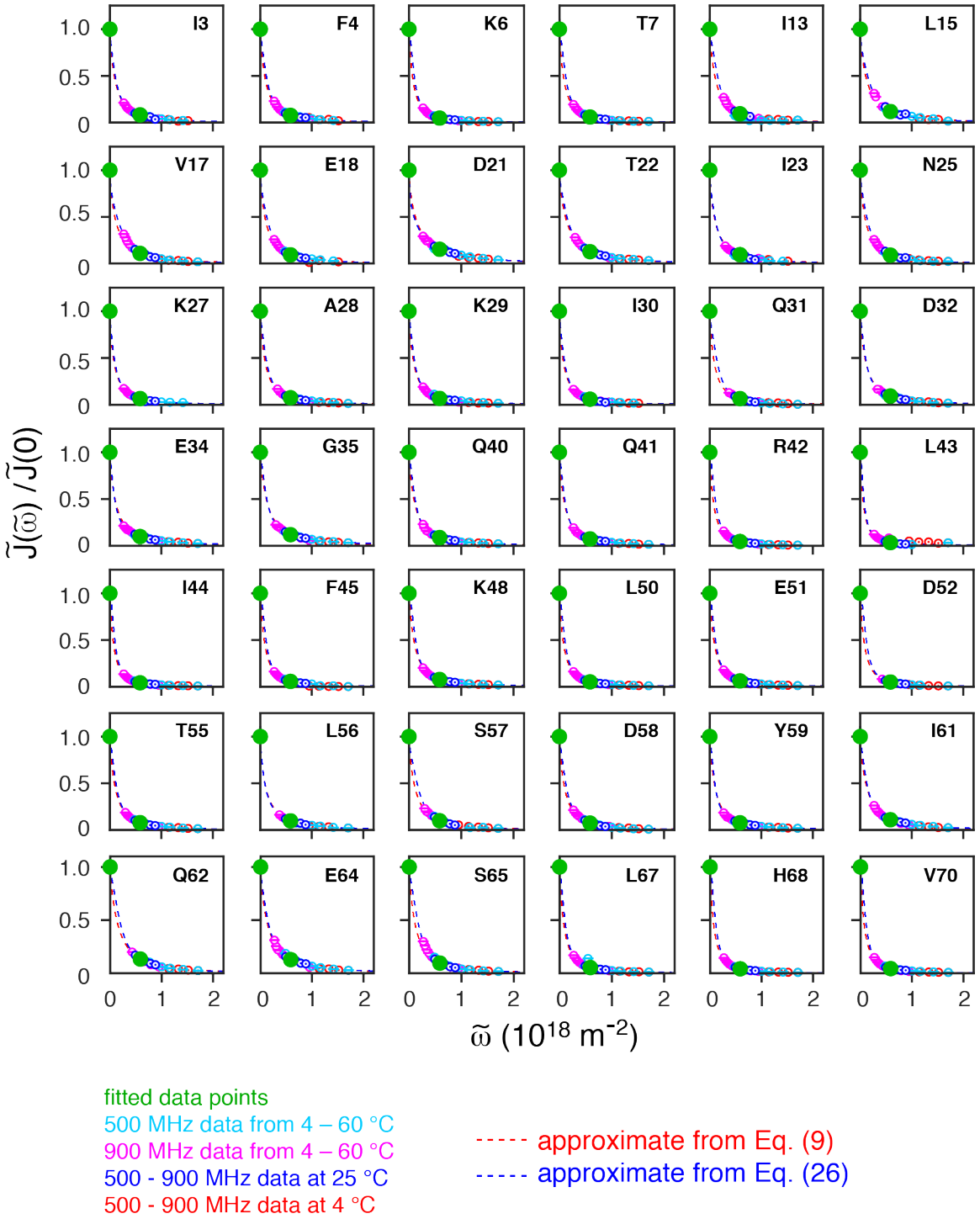

Figure S7. $\tilde{J}(\tilde{\omega})$ for residues of ubiqutin in the presence of 3-carboxy PROXYL using scaling property given by Eq. (22) of the main text. The $\tilde{J}(\tilde{\omega})$ values are obtained from the experimental ^{1}H-Γ_1 values measured over a temperature of 4 to 50 °C at several spectrometer frequencies. The $J(0)$ values were calculated from the experimental ^{1}H-Γ_2 and ^{1}H-Γ_1 values measured at 25 °C and 600 MHz (green filled-in

Figure S7 legend (cont.)

circles). The $J(0)$ and $J(\omega_H)$ values at 600 MHz (green filled-in circles) were used for fitting using Eqs. (9) (red dashed curve) or (26) (blue dashed curve). The magenta and cyan circles represent the $\tilde{J}(\tilde{\omega})$ calculated from the experimental ^{1}H-Γ_1 values measured at 500 and 900 MHz over a temperature range of 4 to 50 °C. The red and blue circles represents the $\tilde{J}(\tilde{\omega})$ calculated from the experimental ^{1}H-Γ_1 values measured at 4 and 25 °C at spectrometer frequencies of 500, 600, 700, 800 and 900 MHz. Note that the red and blue circles overlay almost completely with the magenta and cyan circles, and therefore may not be clearly visible in this plot. The data points that deviate significantly from the scaling property (i.e., the points for which the cyan and magenta circles at 500 and 900 MHz do not overlay) have been removed in these plots.

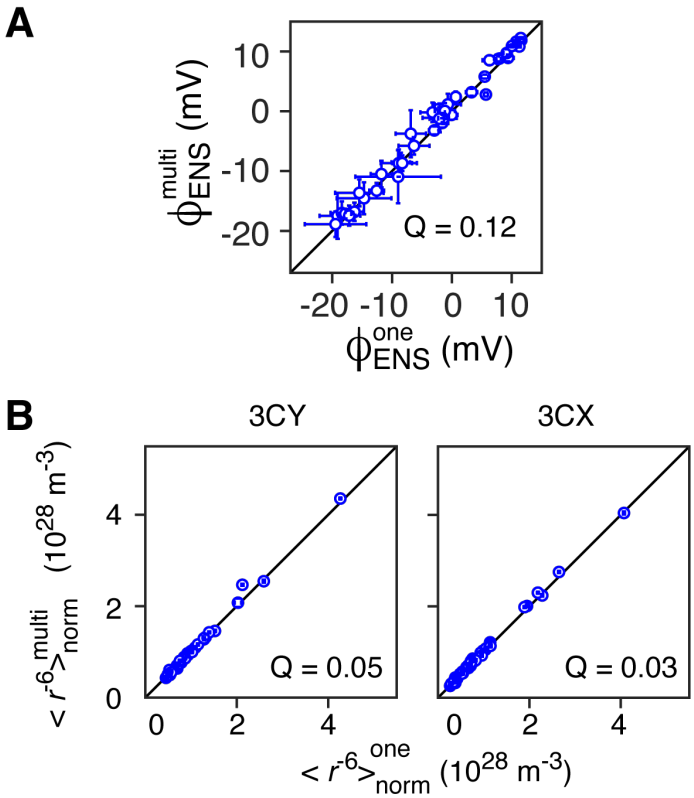

Figure S8. Comparison of ϕ_{ENS} for ubiquitin calculated from one-field versus multiple fields fitting procedures[17] in the presence of 3-carbamoyl PROXYL (3CY) or 3-carboxy-PROXYL (3CX). The $<r^{-6}>_{norm}$ values for 3CY and 3CX were calculated using the one-field or multiple-fields approach, denoted as $\langle r^{-6}\rangle_{norm}^{one}$ and $\langle r^{-6}\rangle_{norm}^{multi}$), respectively, and the corresponding ϕ_{ENS} values, given by $\phi_{ENS} = -\frac{k_B T}{e}\log\left(\frac{\langle r^{-6}\rangle_{norm}(3CY)}{\langle r^{-6}\rangle_{norm}(3CX)}\right)$, are denoted as ϕ_{ENS}^{one} and ϕ_{ENS}^{multi}, respectively. (A) Correlation plot for ϕ_{ENS}^{one} versus ϕ_{ENS}^{multi}. The Q-factor for ϕ_{ENS} was calculated as $Q = \sqrt{\frac{\sum_i \left(\phi_{ENS}^{multi}(i) - \phi_{ENS}^{one}(i)\right)^2}{\sum_i \phi_{ENS}^{multi}(i)^2}}$ where the summation with index i runs over all fields and residues used in the dataset. (B) Correlation between $\langle r^{-6}\rangle_{norm}^{one}$ and $\langle r^{-6}\rangle_{norm}^{multi}$ values for 3CY and 3CX. The Q-factor for $<r^{-6}>_{norm}$ was calculated as $Q = \sqrt{\frac{\sum_i \left(<r^{-6}>_{norm}^{multi)}(i) - <r^{-6}>_{norm}^{one)}(i)\right)^2}{\sum_i <r^{-6}>_{norm}^{multi}(i)^2}}$ where the summation with index i runs over all fields and residues used in the dataset. ^{1}H-Γ_2 and ^{1}H-Γ_1 dataset from 600 MHz at 25 $^\circ$C and the observed relative translational diffusion constants (see Fig. S4) were used for the one-field fitting procedure. $\tilde{J}(0)$ was calculated from ^{1}H-Γ_2 and ^{1}H-Γ_1 at 600 MHz and was used for both one-field and multiple-field fitting. All the available extended spectral densities $\tilde{J}(\tilde{\omega})$ shown in Figs. S6 and S7 were used for the multiple-field fitting procedure.

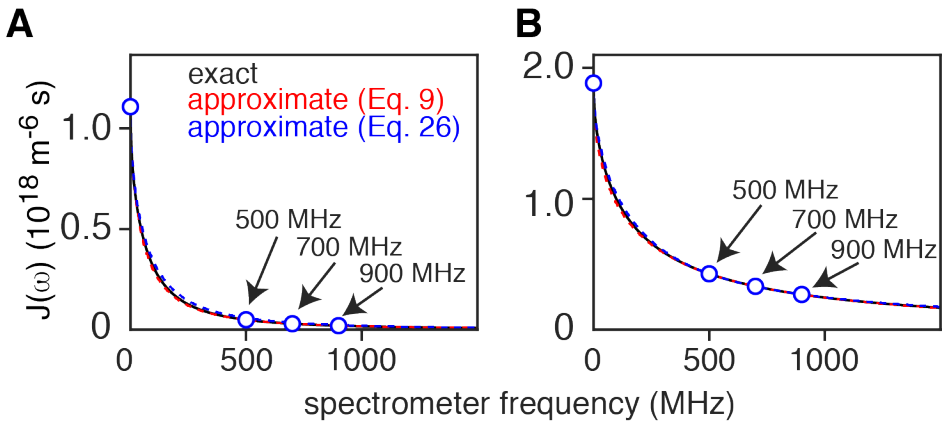

Figure S9. $J(\omega)$ for the force-free hard-sphere (FFHS) model and the corresponding fits using Eqs. (9) and (23) in the main text. The spectral densities were generated using Eqs. (C5) and (D3) with the protein (R_P) and paramagnetic cosolute (R_S) radii set to 16.2 and 3.5 Å, respectively; the contact distance was set to $R_C = R_P + R_S$; $T = 298$ K, $\eta = 0.89$ cp, and $n_S = 1\ m^{-3}$. The spectral densities at spectrometer frequencies of 500, 700 and 900 MHz (blue circles) were used for the fits and the approximate spectral densities given by Eqs. (9) and (26) are shown as dashed red and blue curves, respectively. The distance of the nuclear and electron spins from the protein and paramagnetic cosolute centers, respectively, were set to $p = 0$ Å and $s = 0$ Å in panel A and to $p = 14.8$ Å and $s = 2.0$ Å in panel B. The exact values of $< r^{-6} >_{norm}^{\text{exact}}$ are 5.42×10^{26} m^{-3} in panel A and 4.96×10^{27} m^{-3} in panel B. The approximate $< r^{-6} >_{norm}^{\text{approx}}$ values obtained from Eq. (9) are 5.37×10^{26} m^{-3} in panel A and 4.81×10^{27} m^{-3} in panel B. The approximate $< r^{-6} >_{norm}^{\text{approx}}$ obtained using Eq. (26) are 6.10×10^{26} m^{-3} in panel A and 4.72×10^{27} m^{-3} in panel B.

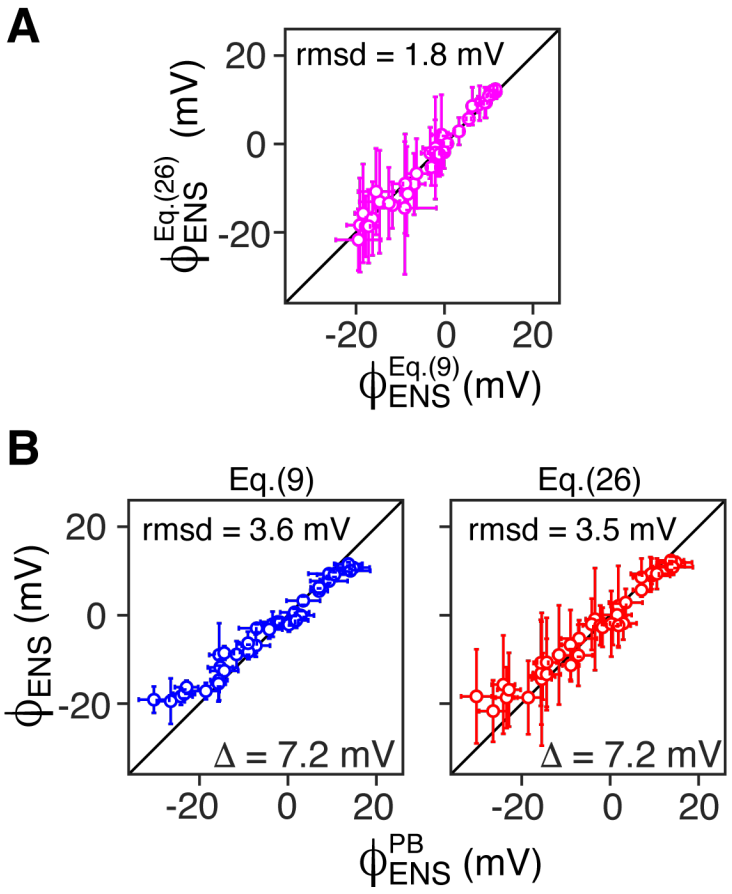

Figure S10. Comparison of ϕ_{ENS} values for ubiquitin calculated from the one-field fitting procedure[17] using Eq. (9) ($\phi_{ENS}^{Eq.(9)}$) and the multiple fields fitting procedure using Eq. (26) ($\phi_{ENS}^{Eq.(26)}$). (A) Correlation plot of $\phi_{ENS}^{Eq.(9)}$ versus $\phi_{ENS}^{Eq.(26)}$. (B) Correlation plot of the theoretical Poisson-Boltzmann ϕ_{ENS}^{PB} potential[18] versus $\phi_{ENS}^{Eq.(9)}$ (left panel) and $\phi_{ENS}^{Eq.(26)}$ (right panel). The values of ϕ_{ENS}^{PB} were shifted vertically by an amount Δ (indicated in the figure) to minimize the root mean square deviation (rmsd) between experimental and theoretical ϕ_{ENS} profiles. The rmsd was calculated as

$$\text{rmsd} = \sqrt{\frac{\sum_i \phi_{ENS}(i) - \phi_{ENS}^{PB}(i)}{n}}$$

where the summation with index i runs over all fields and residues used in the dataset and n is the total number of residues in the dataset. The experimental ^{1}H-Γ_2 and ^{1}H-Γ_1 values measured at 600 MHz at 25 °C, together with the observed relative translational diffusion constants (see Fig. S4) were used for the one-field fitting procedure. $\tilde{J}(0)$ was calculated from ^{1}H-Γ_2 and ^{1}H-Γ_1 at 600 MHz and used for both one-field and multiple-field fittings. All the available extended spectral densities $\tilde{J}(\tilde{\omega})$ shown in Figs. S6 and S7 were used for the multiple-field fitting procedure with Eq. (26).

Supporting Information References

(1) Melchior, A.; Fries, P. H. Local Diffusion in Paramagnetic Solutions by NMR Relaxometry at One Frequency. *J. Am. Chem. Soc.* **2006**, *128*, 7424-7425.

(2) Fries, P. H.; Imbert, D.; Melchior, A. Determination of Outer-Sphere Dipolar Time Correlation Functions from High-Field Nmr Measurements. Example of a Gd^{3+} Complex in a Viscous Solvent. *J. Chem. Phys.* **2010**, *132*, 044502.

(3) Frezzato, D.; Rastrelli, F.; Bagno, A. Nuclear Spin Relaxation Driven by Intermolecular Dipolar Interactions: The Role of Solute−Solvent Pair Correlations in the Modeling of Spectral Density Functions. *J. Phys. Chem. B* **2006**, *110*, 5676-5689.

(4) Solc, K.; Stockmayer, W. Kinetics of Diffusion-Controlled Reaction between Chemically Asymmetric Molecules. I. General Theory. *J. Chem. Phys.* **1971**, *54*, 2981-2988.

(5) Zhou, H.-X.; Szabo, A. Theory and Simulation of the Time-Dependent Rate Coefficients of Diffusion-Influenced Reactions. *Biophys. J.* **1996**, *71*, 2440-2457.

(6) Ferreira, J. C.; Hoskins, R.; Sousa-Pinto, J. *Introduction to the Theory of Distributions*; CRC Press, 1997.

(7) Fries, P. Dipolar Nuclear Spin Relaxation in Liquids and Plane Fluids Undergoing Chemical Reactions. *Mol.Phys.* **1983**, *48*, 503-526.

(8) Fries, P. H. Model-Free Nuclear Magnetic Resonance Study of Intermolecular Free Energy Landscapes in Liquids with Paramagnetic Ln^{3+} Spotlights: Theory and Application to Arg-Gly-Asp. *J. Chem. Phys.* **2012**, *136*, 01B614.

(9) Belorizky, E.; Fries, P. Translational Diffusion in Liquids: Specific Features of the Spectral Densities for Isotropic Intermolecular Interactions. *Chem. Phys. Lett.* **1988**, *145*, 33-38.

(10) Ayant, Y.; Belorizky, E.; Fries, P.; Rosset, J. Effet Des Interactions Dipolaires Magnétiques Intermoléculaires Sur La Relaxation Nucléaire De Molécules Polyatomiques Dans Les Liquides. *J. Phys.* **1977**, *38*, 325-337.

(11) Halle, B. Cross-Relaxation between Macromolecular and Solvent Spins: The Role of Long-Range Dipole Couplings. *J. Chem. Phys.* **2003**, *119*, 12372-12385.

(12) Okuno, Y.; Schwieters, C. D.; Yang, Z.; Clore, G. M. Theory and Applications of Nitroxide-Based Paramagnetic Cosolutes for Probing Intermolecular and Electrostatic Interactions on Protein Surfaces. *J. Am. Chem. Soc.* **2022**, *144*, 21371-21388.

(13) Szabo, A.; Schulten, K.; Schulten, Z. First Passage Time Approach to Diffusion Controlled Reactions. *J. Chem. Phys.* **1980**, *72*, 4350-4357.

(14) Neugebauer, P.; Krummenacker, J. G.; Denysenkov, V. P.; Helmling, C.; Luchinat, C.; Parigi, G.; Prisner, T. F. High-Field Liquid State NMR Hyperpolarization: A Combined DNP/NMRD Approach. *Phys. Chem. Chem. Phys.* **2014**, *16*, 18781-18787.

(15) Bougault, C.; Feng, L.; Glushka, J.; Kupce, E.; Prestegard, J. H. Quantitation of Rapid Proton-Deuteron Amide Exchange Using Hadamard Spectroscopy. *J. Biomol. NMR* **2004**, *28*, 385-390.

(16) Ban, D.; Funk, M.; Gulich, R.; Egger, D.; Sabo, T. M.; Walter, K. F.; Fenwick, R. B.; Giller, K.; Pichierri, F.; de Groot, B. L.; et al. Kinetics of Conformational Sampling in Ubiquitin. *Angew. Chem. Int. Ed. Engl.* **2011**, *50*, 11437-11440.

(17) Okuno, Y.; Szabo, A.; Clore, G. M. Quantitative Interpretation of Solvent Paramagnetic Relaxation for Probing Protein–Cosolute Interactions. *J. Am. Chem. Soc.* **2020**, *142*, 8281-8290.

(18) Okuno, Y.; Schwieters, C. D.; Yang, Z.; Clore, G. M. Theory and Applications of Nitroxide-Based Paramagnetic Cosolutes for Probing Intermolecular and Electrostatic Interactions on Protein Surfaces. *J. Am. Chem. Soc.* **2022**, *144*, 21371-21388.

(19) Ayant, Y.; Belorizky, E.; Fries, P.; Rosset, J. Effet Des Interactions Dipolaires Magnétiques Intermoléculaires Sur La Relaxation Nucléaire De Molécules Polyatomiques Dans Les Liquides. *J. Phys.* **1977**, *38*, 325-337.